electronic stability (no decay correction was applied).

The linear absorption coefficient for Mo Kα is 54.3 cm^{-1}. An empirical absorption correction, using the program DIFABS,[40] was applied which resulted in transmission factors ranging from 0.68 to 1.48. The data were corrected for Lorentz and polarization effects.

The structure was solved by a combination of the Patterson method and direct methods. The non-hydrogen atoms were refined anisotropically. Hydrogen atoms were included in the structure factor calculation in idealized positions (d_{C-H} = 0.95 Å), and were assigned isotropic thermal parameters which were 20% greater than the $B_{equivalent}$ value of the atom to which they were bonded. The final cycle of full-matrix least-squares refinement was based on 3476 observed reflections ($I > 3.00\sigma(I)$) and 235 variable parameters and converged (largest parameter shift was 0.03 times its esd) with unweighted and weighted agreement factors of R = 0.043 and R_w = 0.071.

The standard deviation of an observation of unit weight was 1.80. The weighting scheme was based on counting statistics and include a factor (p = 0.05) to downweight the intense reflections. Plots of $\sum w(|F_o| - |F_c|)^2$ versus $|F_o|$, reflection order in data collection, ($\sin\theta/\lambda$, and various classes of indices showed no unusual trends. The maximum and minimum peaks on the final difference Fourier correspond to 1.09 and −1.16 $e^-/Å^3$, respectively.

Neutral atom scattering factors were taken from Cromer and Waber.[41] Anomalous dispersion effects were included in F_{calc};[42] the values of $\Delta f'$ and $\Delta f''$ were those of Cromer.[41] All calculations were performed using the TEXSAN crystallographic software package of Molecular Structure Corporation.

Crystal Structure of *syn*-Re(C-*t*-Bu)(CH-*t*-Bu)[OCMe(CF$_3$)$_2$]$_2$(THF). Yellow crystals of *syn*-Re(C-*t*-Bu)(CH-*t*-Bu)[OCMe(CF$_3$)$_2$]$_2$(THF) were prepared by cooling a saturated pentane solution. Data were collected on an Enraf-Nonius CAD-4 diffractometer with graphite-monochromated Mo Kα radiation. Of the 7149 reflections which were collected, 6766 were unique (R_{int} = 0.062); equivalent reflections were merged. The intensities of three representative reflections which were measured after every 60 min of X-ray exposure time remained constant throughout data collection time indicating crystal and electronic stability (no decay correction was applied). The data were corrected for Lorentz and polarization effects. The structure was solved by a combination of the Patterson method and direct methods. The final cycle of full-matrix least-squares refinement (TEXRAY Structure Analysis Package, Molecular Structures Corporation (1985)) was based on 3697 observed reflections ($I > 3.00\sigma(I)$) and 343 variable parameters and converged (largest parameter shift was 0.03 times its esd) with unweighted and weighted agreement factors of R = 0.052 and R_w = 0.049. The maximum and minimum peaks on the final difference Fourier correspond to 0.78 and −1.94 $e^-/Å^3$, respectively. The nonhydrogen atoms were refined anisotropically. Crystal data are a = 9.891 (1) Å, b = 17.543 (2) Å, c = 16.570 (2) Å, β = 95.90 (2)°, Z = 4, fw = 759.69, ρ = 1.764 g/cm^3, space group = $P2_1/n$.

Acknowledgment. R.R.S. thanks the National Science Foundation (CHE 88-22508) and R.T. thanks Catalytica Associates, Inc. for a graduate fellowship. We both thank Professor P. Wolczanski for a gift of ((*t*-Bu)$_3$SiOH) and Dr. Vernon Gibson for communicating unpublished results concerning alkoxide exchange in d^0 Mo and W alkylidene complexes.

Supplementary Material Available: ORTEP drawing and a fully labeled drawing for [Re(C-*t*-Bu)(CH-*t*-Bu)(ArNH$_2$)Cl$_2$]$_2$ and *syn*-Re(C-*t*-Bu)(CH-*t*-Bu)[OCMe(CF$_3$)$_2$]$_2$(THF) and a listing of final positional and thermal parameters (14 pages); table of final observed and calculated structure factors (68 pages). Ordering information is given on any current masthead page.

Structural Characterization of Zinc(II) Complexes of Octaethyloxophlorin Dianion and Octaethyloxophlorin Radical Anion

Alan L. Balch,* Bruce C. Noll, and Edward P. Zovinka

Contribution from the Department of Chemistry, University of California, Davis, California 95616. *Received September 16, 1991*

Abstract: The zinc(II) complex of octaethyloxophlorin dianion, Zn^{II}(OEPOH), readily dissolves in pyridine (py) to form red, air-sensitive solutions from which crystalline {(py)Zn^{II}(OEPOH··py)} has been isolated. The X-ray crystal structure reveals the presence of a five-coordinate zinc with an axial pyridine ligand and a planar oxophlorin macrocycle. The meso-hydroxyl substituent is hydrogen bonded to a second pyridine. Oxidation of red pyridine solutions of Zn^{II}(OEPOH) gives green solutions from which crystals of the stable free radical complex {(py)Zn^{II}(OEPO$^\bullet$)}(py) have been isolated. The X-ray crystal structure shows that the zinc(II) ion is five-coordinate with a single axial pyridine ligand. A second, uncoordinated pyridine is trapped on the opposite side of the oxophlorin radical. The structure suffers from inversion disorder as is typical for five-coordinate porphyrin complexes and from disorder of the meso-oxo substituent. The crystal packings of these two closely related substances, which differ only by an electron and a proton, are compared.

Introduction

Relatively little is known about the coordination of metal ions by oxophlorins, **1**, which are porphyrin derivatives that have an

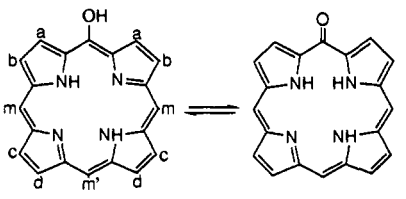

1a **1b**

oxo or hydroxy group at one of the meso positions.[1] Iron oxophlorin complexes are important intermediates in the destruction of porphyrins in vivo in the process catalyzed by heme oxygenase[2] and in vitro in the process of porphyrin oxidation known as coupled oxidation.[3] They are formed by meso-hydroxylation of heme by dioxygen and undergo further attack by dioxygen to eventually form biliverdin as shown in eq 1. An understanding of the chemistry surrounding porphyrin degradation requires further information about the nature of the oxophlorin intermediates.

(1) Clezy, P. S. In *The Porphyrins*; Dolphin, D., Ed.; Academic Press: New York, 1978; Vol. II, p 103.
(2) O'Carra, P. In *Porphyrins and Metalloporphyrins*; Smith, K. M., Ed.; Elsevier: Amsterdam, 1976; p 123.
(3) Bonnet, R.; Dimsdale, M. J. *J. Chem. Soc., Perkin Trans 1* **1972**, 2540.

0002-7863/92/1514-3380$03.00/0 © 1992 American Chemical Society

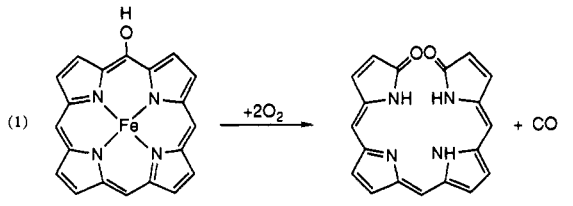

While the oxophlorins bear considerable resemblance to porphyrins, they also have significant differences. Oxophlorins are more readily oxidized to a radical form than are porphyrins.[4,5] The oxophlorins also contain an additional ionizable hydrogen and it is important to be able to specify the nature of the unique meso substituent. That is, is the meso oxygen protonated or deprotonated?

Here we report on the chemical and structural properties of zinc(II) complexes of octaethyloxophlorin (H_2OEPOH, **1**: a, b, c, d = C_2H_5; m, m' = H).[6] These have been examined in order to have adequate models for situations in which the metal ion was redox inactive and would not contribute to the oxidation process that occurs in oxophlorin coordination chemistry.

Results

Properties of Zn^{II}(OEPOH) in Pyridine Solution. The low solubility of Zn^{II}(OEPOH) in organic solvents has hampered previous investigations of its physical properties. For example its low solubility has been cited as a cause for the inability to obtain an ^{1}H NMR spectrum for the complex.[6] Zn^{II}(OEPOH) however does have good solubility in pyridine, and this has facilitated our investigations. Solutions of Zn^{II}(OEPOH) in pyridine show no increase in electric conductivity over that of pure pyridine.

Figure 1 compares the electronic absorption spectra of Zn^{II}(OEPOH) in dichloromethane (trace A) and in pyridine (trace B). This shift in the Soret peak (from 406 nm in dichloromethane to 420 nm in pyridine) and alteration in the lower energy bands are taken to be caused by coordination of pyridine to the zinc and formation of a hydrogen bond between the hydroxyl group and pyridine.

The ^{1}H NMR spectrum of Zn^{II}(OEPOH) in dioxygen-free pyridine is shown in Figure 2. The spectrum shows the meso hydroxy proton at 13.4 ppm and meso protons at 10.3 and 10.1 ppm in a 2:1 intensity ratio. The methylene protons appear as two broad resonances at 4.4 and 4.0 ppm with a 4:12 intensity ratio. The methyl protons produce resonances at 1.9 and 1.7 ppm in a 6:18 intensity ratio. The methyl and methylene resonances at 1.9 and 4.4 ppm are assigned to the ethyl groups that are immediately adjacent to the meso hydroxyl group. The other three ethyl groups (b, c, and d) are insufficiently different magnetically to produce individually resolved resonances. The methyl and methylene resonances are sufficiently broad so that spin–spin splitting is not resolved. The line broadening is attributed to a dynamic process. In the solid (vide infra) the zinc is five-coordinate with one axial pyridine ligand. In solution, the axial pyridine ligand appears to be undergoing rapid exchange. Consequently, the diastereotopic methylene protons are rendered equivalent and these produce broad single resonances. Warming the sample to 25 °C produces only minor changes in the spectrum. The most noticeable is broadening of the hydroxyl resonance.

Crystals of {(py)Zn^{II}(OEPOH··py)} (**2**) are readily obtained by diffusion of methanol into pyridine solutions of Zn^{II}(OEPOH··py) if air is carefully excluded from the sample.

Solutions of Zn^{II}(OEPOH) in pyridine are very susceptible to oxidation by molecular oxygen and other oxidants. Treatment

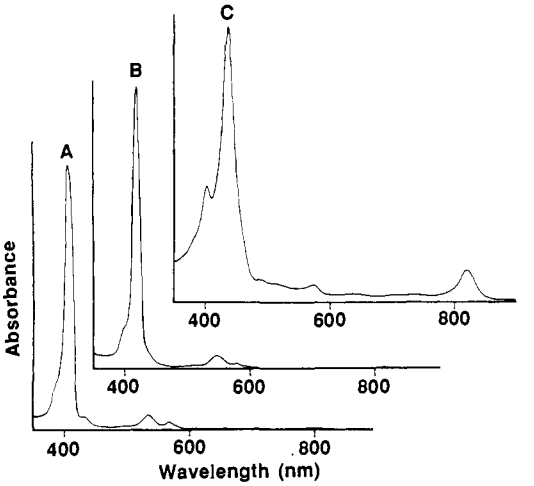

Figure 1. Electronic absorption spectra of: (A) Zn^{II}(OEPOH) in dichloromethane [λ_{max}, nm (ϵ, M^{-1} cm^{-1}): 406 (2.2 × 10^5), 534 (12 700, 568 (6600)]; (B) Zn^{II}(OEPOH) in pyridine [420 (2.8 × 10^5), 546 (16 000), 568 (10 000)]; (C) {(py)Zn^{II}(OEPO•)}(py) in pyridine [404 (51 000), 438 (1.2 × 10^5), 489 (9800), 547 (7500), 637 (3600), 709 (3200), 743 (3300), 819 (14 000)].

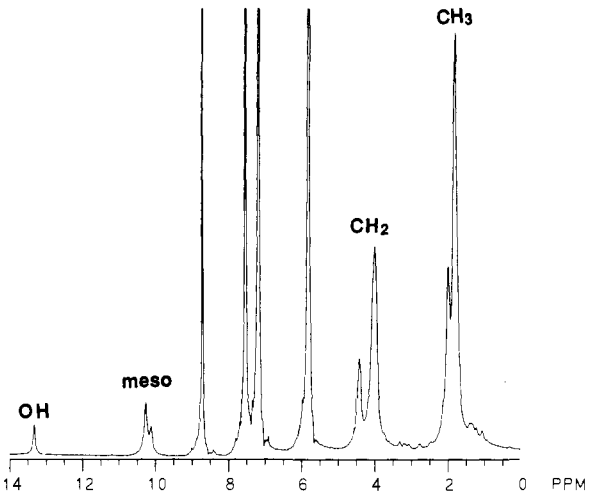

Figure 2. 300-MHz ^{1}H NMR spectrum of Zn^{II}(OEPOH) in pyridine-d_5 at −30 °C.

of such solutions with dioxygen or iodine results in the formation of the radical {(py)Zn^{II}(OEPO•)}. In pyridine solution this oxidation is easily observable because the red solution of Zn^{II}(OEPOH) turns green as the oxidant is added. The free-radical complex, {(py)Zn^{II}(OEPO•)}(py) (**3**), has been obtained in the form of deep red crystals through the diffusion of methanol into an air-saturated pyridine solution of the complex. The electronic absorption spectrum of {(py)Zn^{II}(OEPO•)}(py) in pyridine is shown in trace C of Figure 1. The spectrum shows a characteristic band at 819 nm, a set of weaker absorbances at 743, 709, 637, 570, and 536 nm, and a split Soret peak with maxima at 438 and 404 nm. This spectrum is similar to that reported earlier for the zinc radical complex in *tert*-butyl alcohol or chloroform.[3,4] No ^{1}H NMR spectrum was observable for a sample of {(py)Zn^{II}(OEPO•)}(py) in pyridine solution. However, the electron spin resonance spectrum in dichloromethane solution revealed a sharp signal at g = 2.0, which is characteristic of a free radical species. The magnetic moment of a crystalline sample of {(py)Zn^{II}(OEPO•)}(py) that was redissolved in pyridine at 23 °C is 1.8 (1) μ_B (as determined by the Evans technique[7]). This is consistent with the presence of $S = {}^1/_2$ species.

The infrared spectra of these zinc complexes as mulls in Nujol have been examined. The data are given in the Experimental

(4) Fuhrhop, J.-M.; Besecke, S.; Subramanian, J. *J. Chem. Soc., Chem. Commun.* **1973**, 1.
(5) Fuhrhop, J.-H.; Besecke, S.; Subramanian, J.; Mengersen, C.; Riesner, D. *J. Am. Chem. Soc.* **1975**, *97*, 7141.
(6) Barnett, G. H.; Hudson, M. F.; McCombie, S. W.; Smith, K. M. *J. Chem. Soc. Perkin Trans. 1* **1973**, 691.
(7) Evans, D. F. *J. Chem. Soc.* **1959**, 2003.

Table I. Bond Lengths (Å) and Angles (deg) for {(py)Zn^{II}(OEPOH··py)} (**2**)

Distances							
Zn–N(1)	2.093 (9)	Zn–N(2)	2.064 (8)	C(3)–C(4)	1.445 (14)	C(4)–C(5)	1.358 (16)
Zn–N(3)	2.060 (9)	Zn–N(4)	2.099 (8)	C(4)–C(21)	1.518 (16)	C(5)–C(6)	1.442 (15)
Zn–N(5)	2.183 (8)	N(1)–C(1)	1.376 (14)	C(5)–C(23)	1.507 (14)	C(6)–C(7)	1.395 (17)
N(1)–C(18)	1.353 (13)	N(2)–C(3)	1.390 (15)	C(8)–C(9)	1.454 (17)	C(7)–C(8)	1.393 (15)
N(2)–C(6)	1.388 (13)	N(3)–C(8)	1.378 (13)	C(9)–C(25)	1.498 (14)	C(9)–C(10)	1.356 (14)
N(3)–C(11)	1.378 (15)	N(4)–C(13)	1.353 (15)	C(10)–C(27)	1.519 (17)	C(10)–C(11)	1.456 (16)
N(4)–C(16)	1.363 (13)	N(5)–C(37)	1.328 (12)	C(13)–C(14)	1.473 (14)	C(11)–C(12)	1.394 (14)
N(5)–C(41)	1.337 (14)	N(6)–C(42)	1.333 (18)	C(14)–C(29)	1.501 (16)	C(12)–C(13)	1.395 (16)
N(6)–C(46)	1.310 (14)	O(1)–H(1A)	0.850	C(15)–C(31)	1.509 (14)	C(14)–C(15)	1.364 (16)
O(1)–C(2)	1.392 (14)	C(1)–C(2)	1.387 (14)	C(18)–C(19)	1.462 (16)	C(15)–C(16)	1.452 (15)
C(1)–C(20)	1.489 (15)	C(2)–C(3)	1.392 (15)	C(19)–C(33)	1.503 (14)	C(16)–C(17)	1.394 (16)
Angles							
N(1)–Zn–N(2)	88.1 (3)	N(1)–Zn–N(3)	163.0 (3)	C(4)–C(5)–C(23)	127.3 (10)	C(6)–C(5)–C(23)	124.2 (10)
N(2)–Zn–N(3)	90.2 (3)	N(1)–Zn–N(4)	89.2 (3)	N(2)–C(6)–C(5)	108.7 (10)	N(2)–C(6)–C(7)	124.9 (9)
N(2)–Zn–N(4)	163.1 (3)	N(3)–Zn–N(4)	87.5 (3)	C(5)–C(6)–C(7)	126.4 (9)	N(3)–C(8)–C(9)	110.9 (9)
N(1)–Zn–N(5)	94.8 (3)	N(2)–Zn–N(5)	98.3 (3)	C(6)–C(7)–C(8)	128.3 (10)	C(8)–C(9)–C(10)	106.5 (9)
N(3)–Zn–N(5)	102.1 (3)	N(4)–Zn–N(5)	98.5 (3)	N(3)–C(8)–C(7)	124.0 (11)	C(10)–C(9)–C(25)	126.5 (11)
Zn–N(1)–C(1)	125.3 (6)	Zn–N(1)–C(18)	125.8 (7)	C(7)–C(8)–C(9)	125.1 (9)	C(9)–C(10)–C(27)	128.4 (10)
C(1)–N(1)–C(18)	107.8 (9)	Zn–N(2)–C(3)	127.9 (6)	C(8)–C(9)–C(25)	127.0 (9)	N(3)–C(11)–C(10)	110.7 (9)
Zn–N(2)–C(6)	125.3 (7)	C(3)–N(2)–C(6)	106.8 (8)	C(9)–C(10)–C(11)	106.7 (10)	C(10)–C(11)–C(12)	126.1 (11)
Zn–N(3)–C(8)	126.5 (8)	Zn–N(3)–C(11)	127.8 (6)	C(11)–C(10)–C(27)	124.8 (9)	C(11)–C(12)–C(13)	127.2 (11)
C(8)–N(3)–C(11)	105.1 (9)	Zn–N(4)–C(13)	125.6 (7)	N(3)–C(11)–C(12)	123.2 (10)	N(4)–C(13)–C(12)	125.4 (9)
Zn–N(4)–C(16)	124.9 (7)	C(13)–N(4)–C(16)	108.4 (8)	N(4)–C(13)–C(14)	109.1 (9)	C(12)–C(13)–C(14)	125.5 (11)
Zn–N(5)–C(37)	122.4 (8)	Zn–N(5)–C(41)	120.3 (6)	C(13)–C(14)–C(15)	106.1 (10)	C(13)–C(14)–C(29)	123.6 (10)
C(37)–N(5)–C(41)	117.2 (9)	C(42)–N(6)–C(46)	117.5 (10)	C(15)–C(14)–C(29)	130.2 (9)	C(14)–C(15)–C(16)	107.2 (9)
H(1A)–O(1)–C(2)	112.1 (5)	N(1)–C(1)–C(2)	124.6 (10)	C(14)–C(15)–C(31)	127.2 (10)	C(16)–C(15)–C(31)	125.6 (10)
N(1)–C(1)–C(20)	109.2 (8)	C(2)–C(1)–C(20)	126.1 (10)	N(4)–C(16)–C(15)	109.2 (9)	N(4)–C(16)–C(17)	125.4 (9)
O(1)–C(2)–C(1)	115.5 (9)	O(1)–C(2)–C(3)	115.8 (9)	C(15)–C(16)–C(17)	125.4 (9)	N(1)–C(18)–C(19)	110.1 (9)
C(1)–C(2)–C(3)	128.5 (11)	N(2)–C(3)–C(2)	122.7 (9)	C(16)–C(17)–C(18)	128.1 (10)	C(18)–C(19)–C(20)	107.5 (9)
N(2)–C(3)–C(4)	109.4 (9)	C(2)–C(3)–C(4)	127.9 (11)	N(1)–C(18)–C(17)	125.1 (10)		
C(3)–C(4)–C(5)	106.8 (10)	C(3)–C(4)–C(21)	127.5 (10)	C(17)–C(18)–C(19)	124.7 (9)		
C(5)–C(4)–C(21)	125.6 (9)	C(4)–C(5)–C(6)	108.3 (9)	C(18)–C(19)–C(33)	124.5 (9)		
				C(1)–C(20)–C(19)	105.4 (10)		

Table II. Comparison of Zinc Coordination in Oxophlorin and Porphyrin Complexes

	{(py)Zn^{II}(OEPOH··py)} **2**	{(py)Zn^{II}(OEPO•)}py[a] **3**	{(py)Zn^{II}(OEP)} ref 8	[H$_2$OZn^{II}(OEP•)]$_2$(ClO$_4$)$_2$ ref 18
		Distances, Å		
Zn–N(1)	2.093 (9)	2.092 (3)	2.068 (3)	2.053 (2)
Zn–N(2)	2.064 (8)	2.085 (4)	2.062 (3)	2.049 (2)
Zn–N(3)	2.060 (9)		2.061 (3)	
Zn–N(4)	2.099 (8)		2.075 (3)	
Zn–N(py)	2.183 (8)	2.205 (5)	2.200 (3)	2.141 (3)[b]
Zn–N$_4$	0.31	0.22	0.31	0.24
		Angles, deg		
N(1)–Zn–N(2)	88.1 (3)	88.9 (1)	88.9 (1)	88.80 (9)
N(1)–Zn–N(3)	163.0 (3)	168.1 (1)	164.1 (1)	165.94 (13)
N(1)–Zn–N(4)	89.2 (3)	89.4 (1)	88.7 (1)	89.47 (9)
N(2)–Zn–N(3)	90.2 (3)	90.0 (1)	88.6 (1)	
N(2)–Zn–N(4)	163.1 (3)	168.1 (1)	161.8 (1)	
N(3)–Zn–N(4)	87.5 (3)	89.2 (1)	88.8 (1)	
N(py)–Zn–N(1)	94.8 (3)	93.6 (1)	98.5 (1)	97.03 (7)[b]
N(py)–Zn–N(2)	98.3 (3)	97.7 (2)	101.4 (1)	97.06 (3)[b]
N(py)–Zn–N(3)	102.1 (3)	98.3 (1)	97.5 (1)	
N(py)–Zn–N(4)	98.5 (3)	94.1 (2)	96.8 (1)	
ϕ[c]	8.3	11.5	4	

[a] N(py) is N(c) of Figure 4, N(3) is N(1A), N(4) is N(2A). [b] Distances and angles to oxygen of axial perchlorate. [c] Orientation angle of the axial pyridine and the ZnN$_4$ group.

Section. The clearest differences occur in the O–H stretching region. Both Zn^{II}(OEPOH) and {(py)Zn^{II}(OEPOH··py)} exhibit OH stretching vibrations at 3512 and 3511 cm^{-1}, respectively. In contrast, [(py)Zn^{II}(OEPO•)](py) does not have any features in the 4000–31000 cm^{-1} region. All three samples show complex patterns in the 1670–1500 cm^{-1} region. In this region the most characteristic difference that identifies the radical {(py)Zn^{II}(OEPO•)}(py) is the presence of two strong bands at 1580 and 1527 cm^{-1}. In contrast, the features in the infrared spectra of Zn(OEPOH) and {(py)Zn(OEPOH··py)} in that region are considerably less intense.

Solid State Structure of {(py)Zn^{II}(OEPOH··py)} (2). The structure of {(py)Zn^{II}(OEPOH··py)} has been determined by X-ray crystallography. The asymmetric unit consists of the entire complex molecule which has no crystallographically imposed symmetry. A drawing of the molecule is shown in Figure 3. Selected interatomic distances and angles are presented in Table I.

The zinc ion is five-coordinate with bonds of nearly equal length (av Zn–N, 2.079 Å) to the four pyrrole nitrogens and a longer bond (Zn–N, 2.183 Å) to the axial pyridine. The zinc ion is displaced 0.31 Å out of the N$_4$ plane and positioned toward the axial pyridine. The coordination geometry of the zinc is similar to that found in other zinc porphyrin complexes such as (py)-Zn^{II}(OEP)[8] (OEP is octaethylporphyrin dianion) and for zinc

(8) Cullen, D. L.; Meyer, E. F., Jr. *Acta Crystallogr.* **1976**, *B32*, 2259.

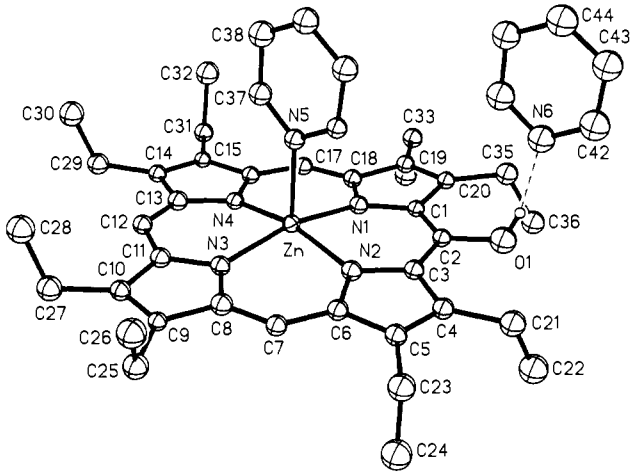

Figure 3. A perspective view of {(py)Zn^{II}(OEPOH··py)} showing 50% contours.

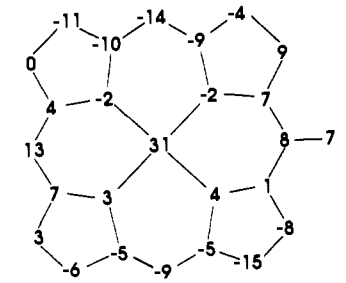

A, {(py)Zn^{II}(OEPOH··py)}

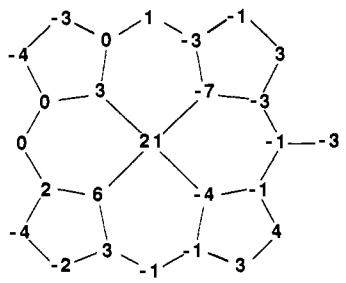

B, {(py)Zn^{II}(OEPO·)}(py)

Figure 4. A diagram of the oxophlorin core for A, {(py)Zn^{II}(OEPOH··py)}, and B, {(py)Zn^{II}(OEPO·)}(py). Each atom symbol has been replaced by a number that represents the perpendicular displacement, in unit of 0.01 Å, from the mean plane of this oxophlorin unit.

complexes of reduced porphyrin (chlorins, etc.) and sterically congested porphyrins.[9-11] Comparative data are given in Table II.

A significant aspect of the structure is the fact that the complex is fully ordered. Porphyrin derivatives with structurally small modifications to their core or periphery are frequently disordered.[12] (For an especially relevant example, continue to the next section.) Likewise, five-coordinate porphyrin complexes frequently suffer from inversion disorder.[13-15] For {(py)Zn^{II}(OEPOH··py)} none

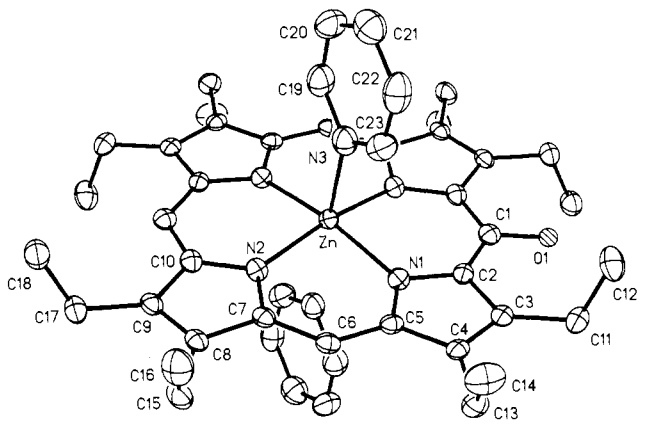

Figure 5. A perspective view of {(py)Zn^{II}(OEPO·)}(py) showing the entire molecule. The alternate positions of the disordered oxygen and zinc atoms are not shown.

of these problems exist. We attribute this to the presence of the second pyridine which is hydrogen bound to the meso hydroxyl group. This additional asymmetry is sufficient to induce order in the solid. Control of hydrogen bonding through cocrystallization with appropriate donors or acceptors[16] is likely to be an important aspect in obtaining ordered forms of other oxophlorin complexes. The oxophlorin ligand in {(py)Zn^{II}(OEPOH··py)} is nearly planar. Figure 4 shows a view of the inner core (with the ethyl groups and pyridine ligands omitted) that shows the displacements of the core atoms from the mean molecular plane.

The hydrogen-bonded portion of the molecule shows characteristic geometry. The N(6)–O(1) distance is 2.702 (15) Å. The hydrogen between them has been identified in the difference electron density map. During refinement, the O–H distance was fixed at 0.85 Å. The resulting N···M distance is 1.87 Å and the O–H···N angle was 164.7°. These parameters are normal for such a hydrogen bonded unit.[17]

Molecular Structure of {(py)Zn^{II}(OEPO·)}(py) (3). The structure of this stable free radical has also been determined by X-ray crystallography. The asymmetric unit consists of half of the molecule which is positioned at a center of symmetry. The structure suffers from two disordered features. One involves the location of the zinc and its relationship to the axial pyridine ligands. The other involves the location of the meso oxo group. Figure 5 shows a drawing of the entire molecule after the disorder that involves the zinc atom is removed.

The presence of the inversion center requires that there is a half atom of zinc located as shown in Figure 5 and a second half-atom located on the opposite side of the porphyrin. This second half-atom is not shown in the drawing. These two half-atoms are too close to one another to be physically reasonable. Consequently the structure is disordered with half of the molecules with the zinc atom and its axial ligand on one side of the porphyrin plane and the other half with the zinc and axial pyridine on the opposite side. As shown by the data in Figure 4, the oxophlorin radical is nearly planar.

In the resolved molecule the zinc ion is five-coordinate and bonded to the four pyrrole nitrogens of the oxophlorin radical anion and to one axial pyridine. Relevant bond lengths and angles involving the zinc coordination are given in Table II. Oxidation produces relatively minor changes in the coordination of the zinc. Its out-of-plane displacement is 0.09 Å less than that for **2** and correspondingly the trans N–Zn–N angles are flattened by 5°.

(9) Spaulding, L. D.; Andrews, L. C.; Williams, G. J. B. *J. Am. Chem. Soc.* **1977**, *99*, 6918.
(10) Barkigia, K. M.; Fajer, J.; Spaulding, L. D.; Williams, G. J. B. *J. Am. Chem. Soc.* **1980**, *103*, 176.
(11) Barkigia, K. M.; Berber, M. D.; Fajer, J.; Medforth, C. J.; Renner, M. W.; Smith, K. M. *J. Am. Chem. Soc.* **1990**, *112*, 8851.
(12) For examples see: Balch, A. L.; Chan, Y. W.; Olmstead, M. M.; Renner, M. W. *J. Am. Chem. Soc.* **1985**, *107*, 2393. Balch, A. L.; Chan, Y. W.; Olmstead, M. M. *J. Am. Chem. Soc.* **1988**, *107*, 6510. Latos-Grażyński, L.; Lisowski, J.; Olmstead, M. M.; Balch, A. L. *J. Am. Chem. Soc.* **1987**, *109*, 4428.
(13) Byrn, M. P.; Curtis, C. J.; Khan, S. I.; Sawin, P. A.; Tsurumi, R.; Strouse, C. E. *J. Am. Chem. Soc.* **1990**, *112*, 1865.
(14) Byrn, M. P.; Strouse, C. E. *J. Am. Chem. Soc.* **1991**, *113*, 2501.
(15) Byrn, M. P.; Curtis, C. J.; Goldberg, I.; Hsiou, Y.; Khan, S. I.; Sawin, P. A.; Tendick, S. K.; Strouse, C. E. *J. Am. Chem. Soc.* **1991**, *113*, 6549.
(16) Etter M. C.; Urbańczyk-Lipkowska, Z.; Zia-Ebrahimi, M.; Panunto, T. W. *J. Am. Chem. Soc.* **1990**, *112*, 8415.
(17) Pauling, L. *The Nature of the Chemical Bond*; Cornell University Press: Ithaca, NY, 1960; p 449.

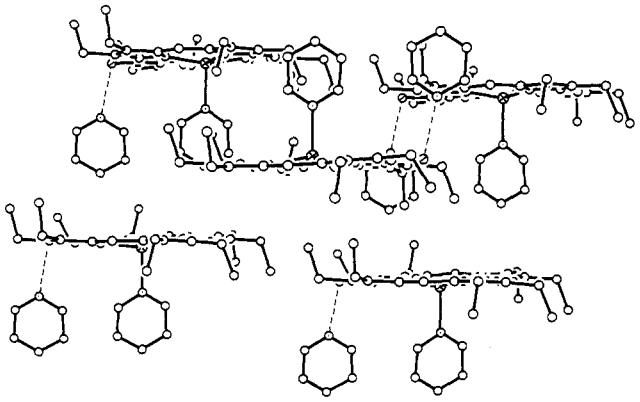

Figure 6. A drawing that shows the solid state of packing of {(py)-Zn^{II}(OEPOH··py)}. Dashed lines show the O–H··N hydrogen bonds.

The Zn–N bond lengths involving the porphyrin and the axial ligand are remarkably similar to the two structures. The coordination geometry can also be compared with that in the five-coordinate zinc–porphyrin radical species, $[H_2OZn(OEP^{\bullet})]ClO_4$.[18] The Zn–N distances in the oxophlorin radical **3** are slightly longer than in the zinc porphyrin radical, but the out-of-plane displacement of the zinc ion is similar. The zinc ion in **3** is not coordinated to the second pyridine that lies on the opposite side of the porphyrin plane. The Zn···N(3a) distance (2.636 (5) Å) is too long to represent a true bond.

The position of the oxo group is also disordered over all four meso carbons. There is 29% occupancy of a site O(1) which is connected to C(1). The presence of the inversion center requires then that there is also 29% occupancy of a corresponding site on the opposite side of the molecule. Additionally there is 21% occupancy of a site (O(1B) connected to C(6). The inversion center also creates 21% occupancy of the site on the fourth meso carbon. Because of this aspect of the disorder, it is impossible to ascertain details regarding the effect of meso substitution and oxidation on the fine structure of the oxophlorin core. Clearly, however, the effects must be small, since the oxo group can be nearly randomly distributed among the four meso positions. The C(1)–O(1) and C(6)–O(1B) distances (1.27 (2) and 1.27 (1) Å, respectively) are significantly shorter than the C(2)–O(1) distance (1.392 (14) Å) in {(py)Zn^{II}(OEPOH··py)}. Thus oxidation is accompanied by shortening and deprotonation of the hydroxyl substituent in the oxophlorin ligand.

Solid-State Molecular Packing of {(py)Zn^{II}(OEPOH··py)} and {(py)Zn^{II}(OEP$^{\bullet}$)}py. It is informative to examine the intermolecular arrangements of these two compounds in the solid state. Their compositions are similar: they differ only by one electron and one proton. Nevertheless their structures are quite different with {(py)Zn^{II}(OEPOH··py)} fully ordered but {(py)Zn^{II}-(OEPO$^{\bullet}$)}py disordered. Figures 6 and 7 show views of the packing of molecules within the solids. The packing in the radical, {(py)Zn^{II}(OEPO$^{\bullet}$)}py, roughly conforms to the body centered cubic lattice that has been carefully analyzed for many tetraphenylporphyrinato complexes ("porphyrin sponges").[11-13] As shown the uncoordinated pyridine molecule occupies what would otherwise be a void in the structure on the side of the oxophlorin radical opposite the axially coordinated pyridine. This is a feature that is common among the "porphyrin sponges" with five-coordinate metal ions.[12] In {(py)Zn^{II}(OEPOH··py)} the situation is quite different. As shown in Figure 6 the axial pyridine and the hydrogen-bond pyridine both protrude from the same face of the oxophlorin. There is no pyridine or other occluded molecule occupying the space opposite the axially coordinated pyridine. The solid in this case is simply constructed from the asymmetric molecular units which have no unusual contacts between one another and no extraneous matter caught in the interstices.

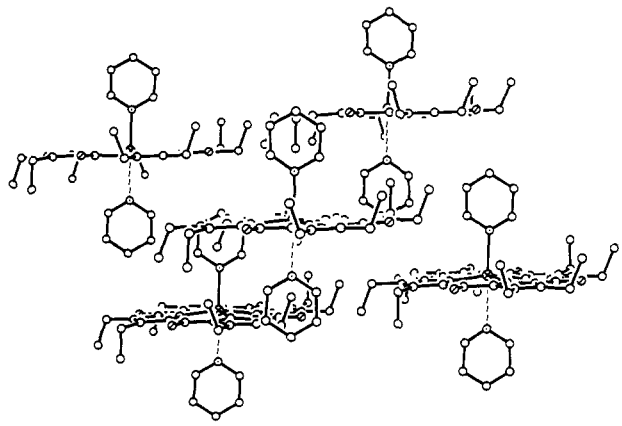

Figure 7. A drawing that shows the solid state of packing of {(py)-Zn^{II}(OEPO$^{\bullet}$)}py. Only one of the two centrosymmetrically related zinc sites is shown as occupied. Dashed lines connect the uncoordinated pyridine to the nearest zinc.

Discussion

The characterization of {(py)Zn^{II}(OEPOH··py)} represents the first example where the metal ion oxidation and ligation state as well as the protonation state of an oxophlorin complex are all thoroughly defined. The ^{1}H NMR spectrum (Figure 2) with the well-resolved hydroxyl proton and the fact that pyridine solutions of Zn^{II}(OEPOH) are nonconductors indicate that this species retains the same protonation state in pyridine solution.

Zn^{II}(OEPOH) is readily oxidized. We have observed the formation of the oxidized radical by electronic absorption spectra and electron spin resonance measurements in both pyridine and dichloromethane, which are representatives of coordinating and noncoordinating solvents. From pyridine solution, the crystalline radical {(py)Zn^{II}(OEPO$^{\bullet}$)}py has been obtained. The geometry of the zinc coordination within this radical is similar to that in the oxophlorin complex and in five-coordinate zinc porphyrins. The macrocyclic ligand in this radical is planar. Most significantly, it shows no evidence for dimerization in the solid state. As seen in Figure 6, each radical exists as an isolated unit with no particularly close approach to any other molecule. In part, the position of the two pyridine molecules serves to insulate the radicals from one another. In contrast, one-electron oxidation of zinc porphyrins produces radicals that show significant pairwise interaction.[18,21] In $[H_2OZn^{II}(OEP^{\bullet})]_2(ClO_4)_2$ this results in the formation of a diamagnetic cofacial π–π dimer with only a 3.31 Å separation between the porphyrin planes (but a 3.7886 (12) Å separation between the zinc ions).[18] For the corresponding radicals formed from zinc tetraarylporphyrins, the core exhibits a saddle-shaped distortion due to twisting of the meso aryl substitutes.[22-24] This twisting allows for the close approach of two of the radicals.

Previously, the infrared spectra of oxophlorin complexes have been somewhat problematic due to difficulties in identifying the OH stretching band.[25,26] This problem may have arisen due to unsuspected oxidation to form the oxophlorin radical with the loss of the hydroxyl proton. When carefully prepared with the exclusion of dioxygen, both Zn^{II}(OEPOH) and {(py)Zn^{II}(OE-POH··py)} show well-defined O–H stretching bands. As is expected, no OH stretch is observed in the radical {(py)Zn^{II}-(OEPO$^{\bullet}$)}(py). This radical shows two rather intense absorptions at 1580 and 1527 cm^{-1}. Complexes containing octaethylporphyrin

(18) Song, H.; Reed, C. A.; Scheidt, W. R. *J. Am. Chem. Soc.* **1989**, *111*, 6867. Song, H.; Orosz, R. D.; Reed, C. A.; Scheidt, W. R. *Inorg. Chem.* **1990**, *29*, 4274.

(19) Fuhrop, J.-H. Mauzerall, D. *J. Am. Chem. Soc.* **1969**, *91*, 4174.

(20) Fajer, J.; Borg, D. C.; Forman, A.; Dolphin, D.; Felton, R. H. *J. Am. Chem. Soc.* **1970**, *92*, 3451.

(21) Fuhrop, J.-H.; Wasser, P.; Riesner, D.; Mauzerall, D. *J. Am. Chem. Soc.* **1972**, *94*, 7996.

(22) Scheidt, W. R.; Lee, Y. J. *Struct. Bonding* **1987**, *64*, 1.

(23) Song, H.; Roth, N. P.; Reed, C. A.; Scheidt, W. R. *Inorg. Chem.* **1989**, *28*, 1839.

(24) Spaulding, L. D.; Eller, P. G.; Bertrand, J. A.; Felton, R. M. *J. Am. Chem. Soc.* **1974**, *96*, 982.

(25) Clezy, P. S.; Liepa, A. J.; Smythe, G. A. *Aust. J. Chem.* **1970**, *23*, 603.

(26) Clezy, P. S.; Nichol, A. W. *Aust. J. Chem.* **1965**, *18*, 1835.

Table III. Crystallographic Data

	{(py)Zn^{II}(OEPOH··py)} (**2**)	{(py)Zn^{II}(OEPO•)}py (**3**)
formula	$C_{46}H_{54}N_6OZn$	$C_{46}H_{53}N_6OZn$
fw	772.3	771.3
color and habit	red plates	dark blocks
crystal system	triclinic	triclinic
space group	$P\bar{1}$ (No. 2)	$P\bar{1}$ (No. 2)
a, Å	9.283 (2)	9.948 (5)
b, Å	14.082 (4)	10.365 (4)
c, Å	15.941 (4)	10.512 (5)
α, deg	101.76 (2)	99.32 (3)
β, deg	93.06 (2)	89.87 (4)
γ, deg	101.09 (2)	114.36 (3)
V, Å^3	1992.7 (9)	972.7 (8)
T, K	130	130
Z	2	1
cryst dimens, mm	0.04 × 0.10 × 0.18	0.66 × 0.40 × 0.36
d_{calcd}, Mg·m^{-3}	1.287	1.317
radiation, Å	Mo Kα (λ = 0.710 69 Å)	Mo Kα (λ = 0.710 69 Å)
μ(Mo Kα), cm^{-1}	6.71	6.87
range of trans factors	0.89–0.98	0.38–0.81
octants collected	$\pm h,\pm k,l$	$\pm h,\pm k,l$
no. of data collected	2423	3430
no. of unique data	2423	3430
no. of data refined	2418 ($F > 6\sigma(F)$)	2827 ($F \geq 4.0\sigma(F)$)
no. of parameters refined	222	246
R^a	0.064	0.061
$R_w{}^a$	0.060 ($w^{-1} = \sigma^2(F) + 0.0003F^2$)	0.063 ($w^{-1} = \sigma^2(F) + 0.0003F^2$)

$^a R = \sum||F_o| - |F_c||/|F_o|$ and $R_w = \sum||F_o| - |F_c||w^{1/2}/\sum|F_o w^{1/2}|$.

radicals show characteristic infrared absorptions of uncertain origin in this region. For example [Fe^{III}Cl(OEP•)](SbCl$_6$) exhibits a prominent absorption at 1535 cm^{-1} [27] while [Zn(OEP•)(H$_2$O)]$_2$(ClO$_4$)$_2$ exhibits weak bands at 1530 and 1555 cm^{-1}.[18] The features at 1580 and 1527 cm^{-1} in **3** may be corresponding features that accompany the formation of an oxophlorin radical. Alternately one may be a carbonyl absorption.

The formation of the crystalline radical {(py)Zn^{II}(OEPO•)}py indicates that molecular oxygen is capable of extracting an electron from Zn^{II}(OEPOH) in solution and that oxygenation does not necessarily proceed further. This observation is an important first step in understanding the nature of oxophlorin reactivity in heme catabolism. It is apparent that the complexed oxophlorin radical is sufficiently stable to resist rapid degradation by molecular oxygen. Further studies of the reactivity of this radical and other oxophlorin radical complexes are in progress.

Experimental Section

Preparation of Compounds. Octaethyloxophlorin and Zn^{II}(OEPOH), infrared (Nujol mull) (cm^{-1}) 3512 m, 1606 m, 1566 m, 1535 w, 1404 w, 1315 w, 1273 m, 1224 m, 1183 m, 1156 m, 1145 m, 1128 w, 1101 m, 1064 m, 1056 s, 1018 s, 957 s, 909 w, 879 w, 832 s, 796 m, 749 w, 727 m, 695 m, were prepared as described previously.[6]

X-ray Data Collection. {(py)Zn^{II}(OEPOH··py)} (**2**). Deep red plates of the complex were obtained by slow diffusion of dioxygen-free methanol into a dioxygen-free pyridine solution of Zn^{II}(OEPOH). Infrared (Nujol mull) (cm^{-1}): 3511 m, 1668 m, 1618 w, 1589 w, 1556 w, 1536 m, 1403 w, 1313 w, 1273 s, 1224 m, 1185 s, 1157 s, 1129 m, 1103 m, 1056 s, 1018 s, 991 w, 956 s, 909 m, 878 m, 831 vs, 796 m, 749 m, 727 s, 695 s. Throughout the process the solution remained red. A suitable crystal was coated with a light hydrocarbon oil and mounted in the 130 K dinitrogen stream of a Siemens R3m/V diffractometer equipped with a locally modified low temperature apparatus. A triclinic unit cell was obtained by indexing reflections from a rotation photograph and verified by examination of axial photographs. Two check reflections showed only random (<2%) variation in intensity during data collection. The data were corrected for Lorentz and polarization effects. Crystal data are collected in Table III.

{(py)Zn^{II}(OEPO•)}py (**3**). Dark red blocks were obtained by slow diffusion of air-saturated methanol into an air-saturated, pyridine solution of Zn^{II}(OEPOH). Infrared (Nujol mull) (cm^{-1}): 1626 w, 1600 w, 1580 s, 1527 s, 1341 m, 1304 m, 1272 s, 1231 m, 1146 w, 1121 m, 1094 s, 1055 m, 1038 m, 1011 ms, 954 s, 908 m, 884 s, 851 w, 800 m, 789 w, 748 m, 694 m. Oxidation was readily observed since the solution acquired the green color characteristic of the dissolved radical. A suitable crystal was coated with a light hydrocarbon oil and mounted in the 130 K dinitrogen stream of a Siemens P2$_1$ diffractometer that was equipped with a locally modified low temperature apparatus. Data collection and handling proceeded as described above with relevant information given in Table III.

Solution and Structure Refinement. Calculations were performed on a DEC VAXstation 3200 with SHELXTL Plus v. 4.00. Scattering factors and corrections for anomalous dispersion were taken from a standard source.[28] The solution for each compound was determined from the Patterson function and subsequent cycles of least-squares refinement and calculation of difference Fourier maps. The asymmetric unit for **2** consists of an entire molecule of the porphyrin with the associated pyridine. Hydrogen H(1A) was located by difference map and fixed at 0.85 Å from O(1) with ideal geometry for subsequent refinement. Other hydrogens were generated using a 0.96 Å C–H vector. All hydrogen thermal parameters were fixed at U = 0.0420 Å^2. An absorption correction was applied.[29] The zinc atom was refined with anisotropic thermal parameters. The goodness-of-fit was 1.33; the mean shift/estimated standard deviation was 0.008 with a maximum of 0.043 for the overall scale. The largest unassigned peak in the final difference map was 0.53 e Å^{-3}.

The zinc atom in **3** is disordered through an inversion center. The asymmetric unit consists of half the zinc oxophlorin radical with a pyridine at full occupancy. The oxygen atom is disordered and occupies each meso position fractionally. Occupancy in the principle sites related by inversion is 29.2% and the occupancy at each alternate site is 20.8%. These site occupancies were refined as dependent variables with a total occupancy of 50% for the asymmetric unit. Hydrogen atoms were generated as described above with a fixed isotropic thermal parameter equal to 0.0260 Å^2. The zinc and nitrogen atoms were refined anisotropically. The goodness-of-fit was 2.13. The mean shift/estimated standard deviation was 0.002 and the maximum was 0.077 for the site occupancy parameter of the oxygen atoms. The largest difference peak had a density of 1.47 e Å^{-3} and was located 0.047 Å from O(1B).

Instrumentation. ^{1}H NMR spectra were recorded on a General Electric QE 300 Fourier transform spectrometer. Electronic spectra were obtained through the use of a Hitachi U-2000 spectrophotometer.

Acknowledgment. We thank the NIH (GM26226) for financial support.

Registry No. 2, 139733-01-0; **3**, 139733-03-2; Zn^{II}(OEPOH), 41114-33-4.

Supplementary Material Available: Tables of bond distances, bond angles, anisotropic thermal parameters, atom positions, and crystal data for {(py)Zn^{II}(OEPOH··py)} and {(py)Zn^{II}(OEPO•)}(py) (20 pages); listings of observed and calculated structure factors (22 pages). Ordering information is given on any current masthead page.

(27) Gans, P.; Buisson, G.; Duêc, E.; Marchon, J.-C.; Erler, B. S.; Scholz, W. F.; Reed, C. A. *J. Am. Chem. Soc.* **1986**, *108*, 1223.

(28) *International Tables for X-ray Crystallography*; Kynoch Press: Birmingham, England, 1974; Vol. 4.

(29) The method obtains an empirical absorption tensor from an expression relating F_o and F_c. Moezzi, B. Ph.D. Thesis, University of California, Davis, 1987.